


Structure of smectic-A liquid crystals in nonuniform domains: Modeling the impact of imperfect boundaries

Ayad S. al Sallo

*School of Computing and Mathematics, University of South Wales, Pontypridd CF37 1DL, United Kingdom*Alan J. Walker *School of Computing, Engineering and Physical Sciences, University of the West of Scotland, Paisley PA1 2BE, United Kingdom*Graeme P. Boswell **School of Computing and Mathematics, University of South Wales, Pontypridd CF37 1DL, United Kingdom*

(Received 15 May 2019; accepted 21 February 2020; published 16 March 2020)

This paper describes the construction of equilibrium configurations for smectic-A liquid crystals subjected to nonuniform physical boundary conditions, with two-dimensional dependence on the director and layer normal, and a nonlinear layer function. Euler-Lagrange equations are constructed that describe key properties of liquid crystals confined between two boundaries exhibiting spatial imperfections. The results of the model are shown to be consistent with previous published findings in simple domains while results are obtained on how the structure of the liquid crystals changes in response to boundary perturbations. Domain sizes are considered representing those currently used in applications while predictions in smaller domains at the limit of current technologies are also made. In particular, it is shown that the curvature along a boundary impacts on the liquid crystal's structure distant from the boundary feature and therefore previously developed mathematical models, that essentially reduced the problem to a single spatial dimension, cannot be used in such circumstances. Consequences for practical applications are briefly discussed.

DOI: [10.1103/PhysRevE.101.032703](https://doi.org/10.1103/PhysRevE.101.032703)

I. INTRODUCTION

Liquid crystals are anisotropic fluids, first discovered in the 19th century by the Austrian botanist Friedrich Reinitzer [1,2]. Most liquid crystals are organic substances that can be induced to exhibit liquid crystal phases by changing either the temperature (thermotropic) or the concentration in a solvent (lyotropic). The most common type of molecule that forms a liquid crystal is an elongated rod-shaped molecule; that is, where one molecular axis is much longer than the other two. This axis is known as the anisotropic axis.

Liquid crystals are classified according to their molecular structure and organization. For example, the nematic phase, where the molecules have no specific positional order but exhibit a common directional alignment known as the director (usually denoted by the unit vector \mathbf{n}) [3, p. 14], has received significant mathematical treatment [3–21]. However, the smectic phase, where the molecules display both positional and orientational order, has received considerably less attention. Specifically, smectic liquid crystals are layered structures with a well-defined interlayer distance, which is in the range 20–80 Å [3, p. 6]. These layers may be described by a scalar function Φ that can be used to investigate layer undulations [22–35] and is often assumed to be of the form $\Phi(x, y, z, t) = x + u(x, y, z, t)$ [or $\Phi(x, y, z, t) =$

$z + u(x, y, z, t)$ depending on the layer orientation], where u denotes layer undulations. However, this ansatz does not accurately describe the underlying features of the smectic layers. Moreover, while there are a number of smectic phases [36, p. 45], this article will focus exclusively on smectic-A, the first discovered and most common of the smectic phases [37, p. 6].

It was previously believed that when the smectic-A phase arose in equilibrium the molecules were aligned in parallel and equidistant layers and where each layer was perpendicular to the director [Fig. 1(a)]. Mathematically, this was represented by assuming the layer normal, denoted by $\mathbf{a} = \nabla\Phi/|\nabla\Phi|$ [3,8,24], was identical to the director \mathbf{n} . However, as hypothesized by de Gennes [8] and later demonstrated by Elston [38], the layer normal and the director can decouple when surface pretilt is applied. Furthermore, Auernhammer *et al.* [39–41], Soddemann *et al.* [42], and Stewart and Stewart [31] indicated that samples of smectic-A under simple shear may exhibit a decoupling between the director \mathbf{n} and the unit layer normal \mathbf{a} .

In order to model this, and other phenomena, Stewart developed a dynamic theory, and a free-energy-density function, for smectic-A liquid crystals [24]. This theory was developed to allow for occurrences in which the director \mathbf{n} and the unit layer normal \mathbf{a} do not always necessarily coincide. The theory was based in part on many of the ideas that were used in the formulation of dynamics for nematics by Ericksen [9,43] and Leslie [10,11,14] and the dynamics for smectic-A by Martin *et al.* [44], de Gennes [45,46], Ahmadi [47], and E [48].

*Corresponding author: graeme.boswell@southwales.ac.uk

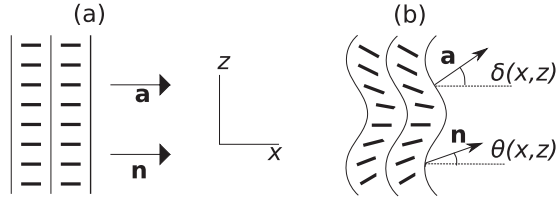


FIG. 1. Planar alignment of smectic-A liquid crystals. (a) In equilibrium, where the director \mathbf{n} is parallel to the smectic layer normal \mathbf{a} and (b) where the director \mathbf{n} does not necessarily coincide with the layer normal \mathbf{a} and each are at angles $\theta(x, z)$ and $\delta(x, z)$, respectively, to the horizontal.

Stewart studied “bookshelf”-aligned smectic-A liquid crystals (so called due to the similarities between the orientation of molecules in adjacent layers in Fig. 1(a) and the spines of books when arranged on bookshelves) with surface pretilt akin to the experimental work of Elston and assumed that the orientation of the smectic layers, and the director, was solely dependent on the in-plane spatial variable [i.e., z in Fig. 1(a)] [25]. When Walker considered the decoupling of the layer normal and the director in cylindrically layered smectic liquid crystals [33], he illustrated that the orientation of the smectic layers and the director may indeed be dependent on both the in-plane spatial variable and the out-of-plane spatial variable (that is, the spatial variable that crosses the smectic layers). Consequently, there is a need to investigate the dependence on the out-of-plane spatial variable in planar samples of smectic-A liquid crystals with uniform and nonuniform cell boundaries. These nonuniform boundaries could account for naturally occurring imperfections in cell boundaries or in circumstances where the smectic layer deformations are used to highlight a foreign body on a cell boundary.

This article considers a smectic-A liquid crystal, arranged in a suite of standard and nonstandard “bookshelf” geometries, where the orientation of the director and layer normal are, and to the authors’ knowledge for the first time, assumed to be functions of both the in- and out-of-plane variables while the layer function is calculated explicitly from the layer normal. Surface pretilt is applied on one or more boundaries, and at the boundaries the smectic layers are assumed to take the orientation of the physical cell wall. A free energy associated with this experiment is created and the corresponding Euler-Lagrange equations are constructed. The Euler-Lagrange equations and the constraint relating the layer function to the layer normal are then integrated numerically. Indeed, due to the complexity of the model equations, this aspect is significantly more challenging than simply including a further spatial dimension into previous investigations. The dependence of the orientation of the director and the layer normal on these spatial variables is shown throughout the samples and the extent to which the director and layer normal decouple is highlighted.

To begin, in Sec. II, we provide the energy density function for the liquid crystal, the associated boundary conditions and construct the standard Euler-Lagrange equations. In Sec. III, a standard “bookshelf”-aligned smectic-A liquid crystal is investigated, where the angles describing the direction of the director and layer normal are assumed to be functions of

both spatial variables. The results are consistent with those of Elston [38] and Stewart [25], validating the solution method developed. Then, in Secs. IV and V, we investigate an array of nonuniform “bookshelf”-aligned smectic-A liquid crystals. The dependence of the layer normal and the director on both spatial variables is illustrated. Comments are made on the results, and possible future work, in Sec. VI.

II. FREE ENERGY AND MINIMIZATION

In this section, we provide the free energy density for a smectic-A liquid crystal. We then proceed to obtain coupled partial differential equations that minimize the free-energy-density function by using the standard Euler-Lagrange equations. This then allows us, in the subsequent sections, to introduce appropriate boundary conditions and solve numerically.

A. Construction of free energy density

We consider a sample of “bookshelf”-aligned smectic-A where the orientation of the director \mathbf{n} and the layer normal \mathbf{a} depend on two spatial variables x and z , as described in Fig. 1(b). The layer normal and director are assumed to make angles $\delta(x, z)$ and $\theta(x, z)$ to the horizontal in the xz plane so that the unit layer normal \mathbf{a} and unit director \mathbf{n} are given by

$$\mathbf{a} = (\cos[\delta(x, z)], 0, \sin[\delta(x, z)]), \quad (1)$$

$$\mathbf{n} = (\cos[\theta(x, z)], 0, \sin[\theta(x, z)]), \quad (2)$$

respectively. When $\delta = \theta = 0$, we have the usual level sets of undisturbed “bookshelf”-aligned smectic-A, i.e., $\mathbf{a} \equiv \mathbf{n} \equiv (1, 0, 0)$, as shown in Fig. 1(a). As is common, a scalar function $\Phi(x, z)$ is introduced, where

$$\mathbf{a} = \frac{\nabla\Phi(x, z)}{|\nabla\Phi(x, z)|}, \quad (3)$$

so that the gradient of $\Phi(x, z)$ describes the local layer structure. The layer normal (1), director (2), and layer function (3) are used to compose an energy density that describes the liquid crystal system. The energy density used by Stewart [24,25], De Vita and Stewart [49], and Walker [33] will be employed here. This energy density is based on the work of Auernhammer *et al.* [39–41], E [48], Ribotta and Durand [50], and Soddemann *et al.* [42] and takes the form

$$w = \frac{1}{2}K_1^a(\nabla \cdot \mathbf{a})^2 + \frac{1}{2}K_1^n(\nabla \cdot \mathbf{n})^2 + \frac{1}{2}B_0(|\nabla\Phi| + \mathbf{n} \cdot \mathbf{a} - 2)^2 + \frac{1}{2}B_1[1 - (\mathbf{n} \cdot \mathbf{a})^2], \quad (4)$$

with the total bulk energy being given by

$$W = \int_V w dV, \quad (5)$$

where V is the sample volume. In the above expression K_1^a is a measure of the bending of the smectic layers, while K_1^n represents the elastic splay deformation of the director \mathbf{n} ; both K_1^a and K_1^n are positive elastic constants with dimensions of force. The constant K_1^a relates to the influence of the orientation of the smectic layers on the total distortion energy. The elastic constant K_1^n is related to K_1 in the usual elastic theory connected with the nematic splay deformation [3,11]. Quantitative measures of these elastic terms have been proposed

to be of the same order of magnitude as the elastic constant K_1 [40], which we shall adopt later. The B_0 term is related to smectic layer compression and its coefficient is an extended version of that known for smectic-A, based on the results in Refs. [8,40,48,50,51], having dimensions of energy per unit volume (N m^{-2}). The fourth term is a measure of the strength of the coupling between \mathbf{a} and \mathbf{n} . The positive constant B_1 has comparable magnitude to B_0 and the same dimensions. We note that in an equilibrium situation this contribution to the energy is minimized when the director and the layer normal are parallel. We also note that alternative energy formulations are possible; for example, the formulation proposed by de Vita and Stewart [52,53] differs in the representation of the layer compression term. Indeed, de Vita and Stewart's energy formulation can be treated using similar methods to those proposed below. It can be seen that the main behavior and characteristics of the solutions are unchanged except in certain key cases [54].

From Eqs. (1) and (3), it follows that

$$\frac{\Phi_{,x}}{|\nabla\Phi|} = \cos[\delta(x, z)], \quad (6)$$

$$\frac{\Phi_{,y}}{|\nabla\Phi|} = 0, \quad (7)$$

$$\frac{\Phi_{,z}}{|\nabla\Phi|} = \sin[\delta(x, z)], \quad (8)$$

where the comma in a subscript indicates the partial derivative with respect to any following variables. From Eq. (7) $\Phi_{,y} = 0$, and while assuming that the layer function is continuously differentiable across the sample, and $\Phi_{,x} \neq 0$ (i.e., $\delta \neq \pi/2$), we can create from (6) and (8) the partial differential equation

$$\Phi_{,z} - \Phi_{,x} \tan[\delta(x, z)] = 0. \quad (9)$$

This equation, and its cylindrical coordinate counterparts, was investigated by Walker [33,34], where the angles that describe the orientation of the layers and the director were assumed to be functions of the in-plane spatial variable only. In those cases, the method of characteristics provided an analytical solution for the layer function Φ , and the free energy was minimized using the standard Euler-Lagrange equations. However, due to the nature of the nonlinear boundary conditions to be applied in this work, we retain the dependence of the layer normal and the director on both spatial variables. Consequently there is no simple analytical solution to Eq. (9) and hence we seek an alternative numerical solution.

Using (9), and to be consistent with Eq. (6), $|\nabla\Phi|$ can be expressed as

$$|\nabla\Phi| = \Phi_{,x} \sec \delta(x, z). \quad (10)$$

Consequently, using Eqs. (1), (2), (4), and (10), we may write the nonlinear free energy of the system to be

$$w = \frac{1}{2}K_1^a(\delta_{,z} \cos \delta - \delta_{,x} \sin \delta)^2 + \frac{1}{2}K_1^n(\theta_{,z} \cos \theta - \theta_{,x} \sin \theta)^2 + \frac{1}{2}B_0[\Phi_{,x} \sec \delta + \cos(\theta - \delta) - 2]^2 + \frac{1}{2}B_1 \sin^2(\theta - \delta). \quad (11)$$

We are now required to minimize this free-energy function in order to consider the equilibrium forms of the layer normal and the director.

B. Minimization of free energy

The minimization of the energy density function in Eq. (11) can be investigated by using the Euler-Lagrange equations

$$\frac{\partial w}{\partial \theta} - \frac{\partial}{\partial x} \left(\frac{\partial w}{\partial \theta_{,x}} \right) - \frac{\partial}{\partial z} \left(\frac{\partial w}{\partial \theta_{,z}} \right) = 0, \quad (12)$$

$$\frac{\partial w}{\partial \delta} - \frac{\partial}{\partial x} \left(\frac{\partial w}{\partial \delta_{,x}} \right) - \frac{\partial}{\partial z} \left(\frac{\partial w}{\partial \delta_{,z}} \right) = 0, \quad (13)$$

$$\frac{\partial w}{\partial \Phi} - \frac{\partial}{\partial x} \left(\frac{\partial w}{\partial \Phi_{,x}} \right) - \frac{\partial}{\partial z} \left(\frac{\partial w}{\partial \Phi_{,z}} \right) = 0, \quad (14)$$

resulting in the following three coupled partial differential equations:

$$0 = K_1^n(\theta_{,z} \cos \theta - \theta_{,x} \sin \theta)(-\theta_{,z} \sin \theta - \theta_{,x} \cos \theta) - B_0 \sin(\theta - \delta)[\Phi_{,x} \sec \delta + \cos(\theta - \delta) - 2] + B_1 \sin(\theta - \delta) \cos(\theta - \delta) + K_1^n[\sin \theta(\theta_{,z} \cos \theta - \theta_{,x} \sin \theta)]_{,x} - K_1^n[\cos \theta(\theta_{,z} \cos \theta - \theta_{,x} \sin \theta)]_{,z}, \quad (15)$$

$$0 = K_1^a(\delta_{,z} \cos \delta - \delta_{,x} \sin \delta)(-\delta_{,z} \sin \delta - \delta_{,x} \cos \delta) + B_0[\Phi_{,x} \sec \delta + \cos(\theta - \delta) - 2] \times [\Phi_{,x} \sec \delta \tan \delta + \sin(\theta - \delta)] - B_1 \sin(\theta - \delta) \cos(\theta - \delta) + K_1^a[\sin \delta(\delta_{,z} \cos \delta - \delta_{,x} \sin \delta)]_{,x} - K_1^a[\cos \delta(\delta_{,z} \cos \delta - \delta_{,x} \sin \delta)]_{,z}, \quad (16)$$

$$0 = \{B_0 \sec \delta[\Phi_{,x} \sec \delta + \cos(\theta - \delta) - 2]\}_{,x}. \quad (17)$$

Following previous techniques [24,33], the above Euler-Lagrange equations (15)–(17) are nondimensionalized by introducing

$$\lambda = \sqrt{\frac{K_1^n}{B_0}}, \quad \kappa = \frac{K_1^a}{K_1^n}, \quad B = \frac{B_1}{B_0}, \quad \bar{\Phi} = \frac{\Phi}{\lambda}, \quad \bar{z} = \frac{z}{\lambda}, \quad \bar{x} = \frac{x}{\lambda}, \quad (18)$$

where λ is a molecular length scale [8, p. 344]. The compression constant B_0 typically takes a value of the order 10^6 N m^{-2} , while the elastic splay deformation parameter K_1^n typically takes a value of the order 10^{-12} N [24,33]. Consequently, the molecular length scale λ is of the order of 10^{-9} m (10 \AA) which is comparable to the smectic layer thickness ($20\text{--}80 \text{ \AA}$), as stipulated by de Gennes [8]. In the above nondimensionalization, κ is a measure of the elastic properties of the liquid crystal, with its magnitude playing a particular role in the reorientation of the smectic layers in previous research, while the constant B is a relative measure of the layer compression constant and the strength of the coupling between the layer normal and the director and it, too, has shown significant influence in the reorientation of the smectic layers in previous research [24,33]. Consistent with other investigations [25], it is assumed that B_1 and K_1^a take values with approximately similar orders of magnitude to B_0 and K_1^n , respectively, and hence, for the purpose of a thorough investigation, B and κ will accordingly take values between 10^{-3} and 10^3 .

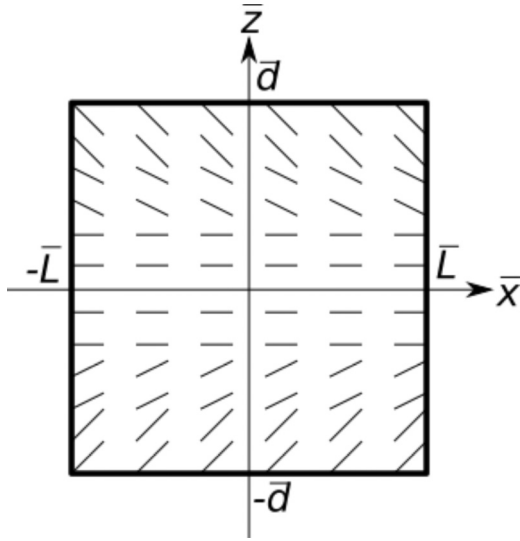


FIG. 2. Planar alignment of smectic-A liquid crystals in a regular rectangular domain with pretilt applied on boundaries $\bar{z} = \pm \bar{d}$ and periodic conditions on $\bar{x} = \pm \bar{L}$ as described in the text.

Consequently, the Euler-Lagrange equations (15)–(17) now reduce to

$$0 = (\theta_{,\bar{z}} \cos \theta - \theta_{,\bar{x}} \sin \theta)(-\theta_{,\bar{z}} \sin \theta - \theta_{,\bar{x}} \cos \theta) - \sin(\theta - \delta)[\bar{\Phi}_{,\bar{x}} \sec \delta + \cos(\theta - \delta) - 2] + B \sin(\theta - \delta) \cos(\theta - \delta) + [\sin \theta (\theta_{,\bar{z}} \cos \theta - \theta_{,\bar{z}} \sin \theta)]_{,\bar{x}} - [\cos \theta (\theta_{,\bar{z}} \cos \theta - \theta_{,\bar{x}} \sin \theta)]_{,\bar{z}}, \quad (19)$$

$$0 = \kappa (\delta_{,\bar{z}} \cos \delta - \delta_{,\bar{x}} \sin \delta)(-\delta_{,\bar{z}} \sin \delta - \delta_{,\bar{x}} \cos \delta) + [\bar{\Phi}_{,\bar{x}} \sec \delta + \cos(\theta - \delta) - 2] \times [\bar{\Phi}_{,\bar{x}} \sec \delta \tan \delta + \sin(\theta - \delta)] - B \sin(\theta - \delta) \cos(\theta - \delta) + \kappa [\sin \delta (\delta_{,\bar{z}} \cos \delta - \delta_{,\bar{x}} \sin \delta)]_{,\bar{x}} - \kappa [\cos \delta (\delta_{,\bar{z}} \cos \delta - \delta_{,\bar{x}} \sin \delta)]_{,\bar{z}}, \quad (20)$$

$$0 = [\bar{\Phi}_{,\bar{x}} \sec \delta + \cos(\theta - \delta) - 2]_{,\bar{x}}. \quad (21)$$

The solutions of Eqs. (19)–(21) correspond to the minimization of the energy function (11). Clearly, there is no nontrivial analytical solution to the above equations. However, insightful numerical solutions are sought for a suite of problems with various applied boundary conditions in the following sections.

III. UNIFORM BOUNDARY CONDITIONS

We first reconsider the set-up investigated experimentally by Elston [38] and analytically by Stewart [25]. That is, “bookshelf”-aligned smectic-A liquid crystals confined between two parallel glass plates, a distance $2d = 2\bar{d}\lambda$ units apart, as described in Fig. 2. Surface pretilt of the director is applied so that $\theta(\bar{x}, -\bar{d}) = -\theta(\bar{x}, \bar{d}) = \theta_0$ and it will also be assumed that the smectic layers will exhibit a fixed layer tilt at the boundaries, so that $\delta(\bar{x}, -\bar{d}) = -\delta(\bar{x}, \bar{d}) = \delta_0$. Periodic conditions are applied on the fictitious $\bar{x} = -\bar{L}$ and $\bar{x} = \bar{L}$ boundaries, i.e., $\theta(-\bar{L}, \bar{z}) = \theta(\bar{L}, \bar{z})$ and $\delta(-\bar{L}, \bar{z}) = \delta(\bar{L}, \bar{z})$.

The model equations (19) and (20) were solved numerically using COMSOL Multiphysics [55], which uses the method of finite elements by constructing a suitable triangular mesh over the domain. The constraint (9) was imposed in the numerical scheme, via COMSOL’s model builder. Postsolution testing showed that the magnitude of the left-hand side of (9) to not exceed 10^{-12} , while generally falling between 10^{-16} and 10^{-14} .

Previous investigations on smectic-A liquid crystal structure in a single spatial dimension have shown that nonzero boundary conditions induce a boundary layer region in which the director and layer normal attempt to align [24,25,33,49]. In anticipation of similar effects in this higher spatial dimension investigation, boundary layers are incorporated into the upper and lower surfaces of the domains by refining the mesh on the corresponding boundaries. In all numerical solutions, the mesh resolution was selected so that further mesh refinement produced graphically indistinguishable results. The numerical routines utilized by COMSOL require initial values for the model variables to be defined from which the final solution is constructed. Crucially, the efficiency of the method was seen to depend on the choice of these initial values. Provided the initial values satisfied the boundary conditions for θ and δ at $\bar{z} = \pm \bar{d}$, COMSOL was usually able to iterate the initial distributions so that these iterations converged rapidly to the final equilibrium configuration. As expected, the convergence was observed to be fastest when the initial values were chosen to be “close” to the equilibrium solution. Therefore, by exploiting known results for the single spatial configuration in a standard “bookshelf” geometry [25], initial values of θ and δ were selected to be zero for $\bar{z} \in [-\bar{d} + 1, \bar{d} - 1]$ and changing linearly outwith this region to take the specified values at $\bar{z} = \pm \bar{d}$ and so displaying similar characteristics to the solutions in Ref. [25], namely steep changes in the director and layer normal angles close to the boundary and values close to zero elsewhere. The initial value of Φ was taken to be unity throughout the domain. It should be noted that the solutions of the above Euler-Lagrange equations correspond to local energy minimizers. Hence there is a risk that the numerical iterations converge on a local minimizer, but not necessarily the global energy minimizer. To mitigate against this possibility, alternative initial iterates also satisfying the boundary conditions were considered in an attempt to obtain different local minimizers but in all cases the numerical iterates converged on the same solution.

With the above choice of initial values and running on a desktop computer with an Intel Core i7 processor with 6 GB of RAM, the computational times for the domains described in this investigation were typically between 1 and 2 min.

Typical values obtained for $\theta(\bar{x}, \bar{z})$ and $\delta(\bar{x}, \bar{z})$ and their difference $\theta(\bar{x}, \bar{z}) - \delta(\bar{x}, \bar{z})$ are shown in Fig. 3 for a range of domains corresponding to $10 \text{ nm} \times 10 \text{ nm}$ ($\bar{d} = \bar{L} = 5$), $0.1 \mu\text{m} \times 0.1 \mu\text{m}$ ($\bar{d} = \bar{L} = 50$), and $1 \mu\text{m} \times 1 \mu\text{m}$ ($\bar{d} = \bar{L} = 500$), therefore representing current typical liquid crystal technologies along with potential future scenarios [38]. While smaller domains can be considered from a purely mathematical perspective, from a physical perspective the continuum approach would cease to be valid in such circumstances. Notice that the director angle $\theta(\bar{x}, \bar{z})$ and layer normal angle $\delta(\bar{x}, \bar{z})$ appear independent of the variable \bar{x} and hence their

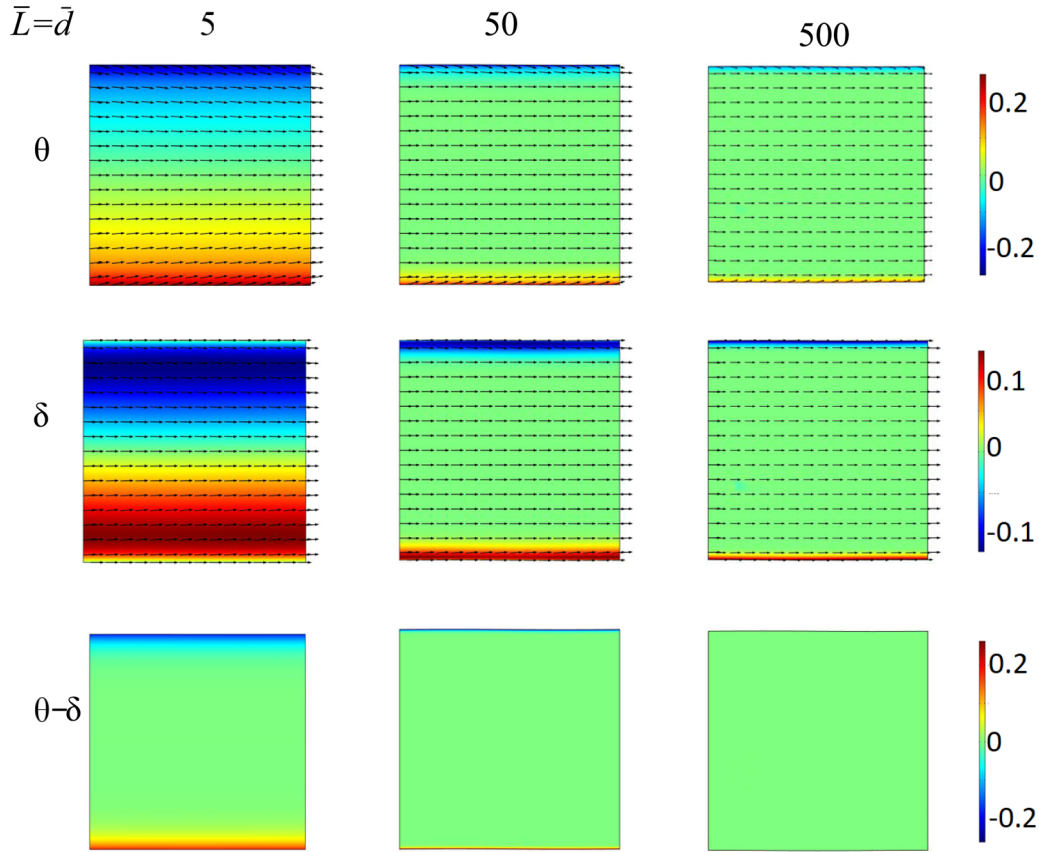


FIG. 3. Solutions of model equations (19) and (20) for different domain sizes with $B = \kappa = 1$ in a rectangular domain using boundary conditions as described in text with $\theta_0 = \pi/12$ and $\delta_0 = 0$. Arrows indicate the director and layer normal vectors where appropriate.

alignment depends only on the spatial variable \bar{z} . Indeed, this independence was confirmed numerically in COMSOL since the computed values of $\theta_{,\bar{x}}(\bar{x}, \bar{z})$ and $\delta_{,\bar{x}}(\bar{x}, \bar{z})$ had absolute values less than 10^{-6} throughout all the domains compared to $\theta_{,\bar{z}}(\bar{x}, \bar{z})$ and $\delta_{,\bar{z}}(\bar{x}, \bar{z})$ which had maximum values of orders between 10^0 and 10^1 . In all cases, the value of the director angle θ declined from its value θ_0 at the boundary $\bar{z} = -\bar{d}$ (or increased from $-\theta_0$ at $\bar{z} = \bar{d}$) to take a value close to zero typically within 5–10 spatial units from the boundaries. The layer normal angle increased from δ_0 on the $\bar{z} = -\bar{d}$ boundary (or decreased from $-\delta_0$ on the $\bar{z} = \bar{d}$ boundary) to take the same value as the director angle, usually within 2 spatial units. Thus, and as in Ref. [25], there are typically two boundary layers; the first where the director and layer normal mutually align, and the second where both simultaneously reorient to zero.

The manner of the alignment between the director and layer normal can be more easily compared by considering their orientation along a single layer (i.e., a given value of \bar{x}), thereby allowing a direct comparison with the studies of Elston [38] and Stewart [24]. The resultant alignment depends on the values of the model parameters B and κ in the same manner obtained by Elston [38] and Stewart [24]. Figure 4 illustrates typical values of $\theta(\bar{x}, \bar{z})$ and $\delta(\bar{x}, \bar{z})$ along the layer $\bar{x} = 0$ where a logarithmic scale in terms of the distance from the $\bar{z} = -\bar{d}$ boundary has been adopted to fully illustrate the convergence properties between the layer normal

and director angles away from a boundary where pretilt has been applied. Notice that for $\kappa < 1$, the layer normal angle δ increases to the director angle θ in a region close to the boundary while θ declines to δ in the instance of $\kappa > 1$; this behavior is consistent with the definition of $\kappa = K_1^a/K_1^n$, where K_1^a and K_1^n denote the desire of δ and θ , respectively, to change over a spatial interval. Additionally, as B is increased, the director and layer normal angles converge over a shorter spatial distance before both tend to zero away from the boundary, consistent with B representing the coupling between the layer normal and director vectors. (Note that due to the symmetry embedded in the model equations and imposed through the boundary conditions, similar behavior is observed around the $\bar{z} = \bar{d}$ boundary, albeit with the signs of the angles reversed.) Consequently, we deduce that a key prediction of those previous investigations, namely that there are no interlayer effects for smectic liquid crystals in a bookshelf geometry, is indeed valid. However, when the boundaries of the domain are perturbed, the “bookshelf” geometry no longer applies and far more complex behavior is possible, as we now investigate.

IV. NONUNIFORM BOUNDARY CONDITIONS

The uniform boundary conditions investigated above demonstrated that the standard “bookshelf” geometry considered in previous investigations is indeed a suitable approach

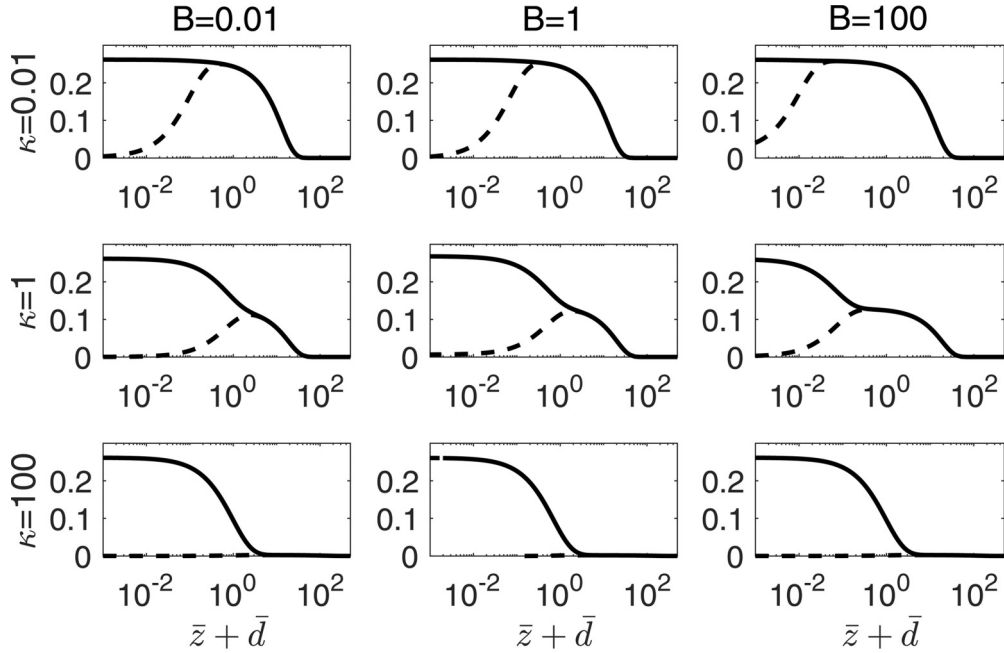


FIG. 4. Solutions of model equations (19) and (20) in a rectangular domain with $\bar{d} = \bar{L} = 500$ and for different values of B and κ using boundary conditions as described in text with $\theta_0 = \pi/12$ and $\delta_0 = 0$ along the layer $\bar{x} = 0$, where θ and δ are shown by the solid and dashed lines, respectively. The horizontal axes utilize a logarithmic scale of the distance from the lower surface, i.e., $\bar{z} + \bar{d}$.

for such domains and also that the minimization approach outlined in Sec. II coupled with the numerical solution method provides consistent results. However, de Gennes states that “the notion of a perfectly flat or locally smooth surface is an *ad hoc* idealization” [8, p. 353] and hence we must take into account the possibility of undulations in the surfaces and surface dislocation densities. Consequently, the validity of the standard “bookshelf” approach requires investigation in such settings. To this end, we now consider a suite of smectic-*A* samples confined between nonuniform boundaries, as schematically illustrated in Fig. 5. In this article, we have restricted our attention to nonuniform boundaries having cyclic perturbations, similar to that of de Gennes [8]. This allows us to consider the possibility of warped physical boundaries through possible manufacturing defects, heat distortions, or poor treatment. We investigate the effect that the boundaries have on the realignment of the layer normal

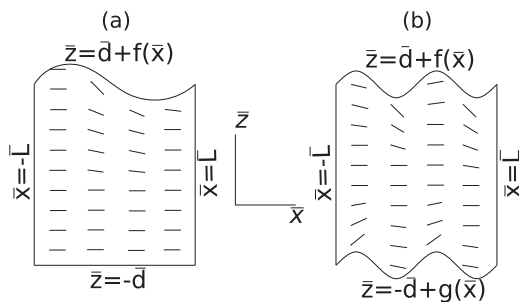


FIG. 5. Planar alignment of smectic-*A* liquid crystals; (a) configuration (I) with one nonuniform boundary displaying a cyclic perturbation, (b) configuration (II) with two nonuniform boundaries having cyclic perturbations (that may be out of phase).

and the director, and show the differences compared uniform boundary conditions.

To isolate the effect of perturbations at the boundaries on the director and layer alignments, we consider the equilibrium configurations that minimize the energy function (11) in a semirectangular region in the xz plane bounded by $\bar{x} = -\bar{L}$ (representing the (fictitious) left side of the domain), $\bar{x} = \bar{L}$ (representing the (fictitious) right side of the domain), $\bar{z} = \bar{d} + f(\bar{x})$ (representing the top of the domain), and $\bar{z} = -\bar{d} + g(\bar{x})$ (representing the bottom of the domain), where \bar{L} and \bar{d} are as defined in Sec. III. To investigate the effect of different types of perturbations on the layer structure at the upper and lower boundaries, two different configurations were considered (see Fig. 5):

(I) $f(\bar{x}) = \bar{A} \sin[\pi(\bar{x} + \bar{L})/\bar{L}]$, $g(\bar{x}) = 0$, representing a cyclic perturbation on one boundary only [Fig. 5(a)],

(II) $f(\bar{x}) = \bar{A} \sin[n\pi(\bar{x} + \bar{L})/\bar{L}]$, $g(\bar{x}) = \bar{A} \sin[n\pi(\bar{x} + \bar{L})/\bar{L} + \omega]$, representing cyclic perturbations on both boundaries [Fig. 5(b)],

where in each instance $\bar{A} < \bar{d}$ represents the maximum magnitude of the perturbations, the integer n denotes the frequency of oscillations and ω the phase shift between boundaries in the second configuration. Periodic boundary conditions were applied to the layer normal angle δ and the director angle θ on the $\bar{x} = \pm\bar{L}$ boundaries as described previously, i.e., $\theta(-\bar{L}, \bar{z}) = \theta(\bar{L}, \bar{z})$ and $\delta(-\bar{L}, \bar{z}) = \delta(\bar{L}, \bar{z})$. Surface pretilt was applied to the upper and lower boundaries through fixed boundary conditions that specified the director and layer normal *relative to the boundary*. Thus on the upper surface $\bar{z} = \bar{d} + f(\bar{x})$, the director angle θ was set to be $\tan^{-1}[f'(\bar{x})] - \theta_0$ and the layer normal angle was set to be $\tan^{-1}[f'(\bar{x})] - \delta_0$ for specified values of θ_0 and δ_0 . This choice of boundary condition is consistent with previous studies on uniform

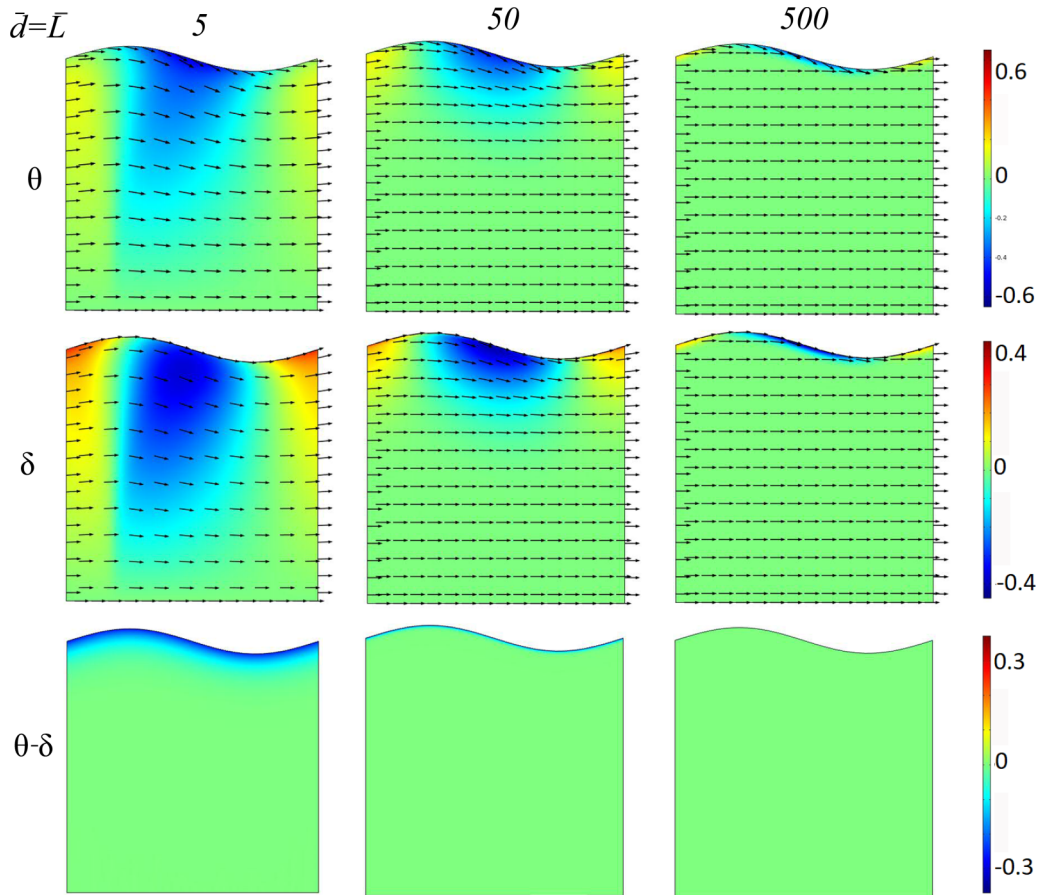


FIG. 6. Solutions of model equations (19) and (20) in configuration (I) of Fig. 5(a) $B = \kappa = 1$ and $\bar{A} = 0.1\bar{d}$ using boundary conditions as described in text with $\theta_0 = \pi/12$ and $\delta_0 = 0$ for domain sizes as indicated.

domains [24,33]. Depending on the geometry of the domain, different boundary conditions were used on the lower surface. In configuration (I) [i.e., Fig. 5(a)] where $g(\bar{x}) = 0$, both θ and δ were set to be zero on $\bar{z} = -\bar{d}$. In configuration (II), similar conditions to those applied on the upper surface were used on the lower boundary except the director and layer normal angles were reflected with respect to the boundary; specifically θ and δ were taken to be $\tan^{-1}[g'(\bar{x})] + \theta_0$ and $\tan^{-1}[g'(\bar{x})] + \delta_0$, respectively, again consistent with previous studies.

Model equations (19) and (20) with constraint (9) were solved using the boundary conditions as described above using the same method developed in Sec. III.

A. Configuration (I)

The numerical solution with $B = \kappa = 1$ for the configuration shown in Fig. 5(a) with the same range of values of \bar{L} and \bar{d} used previously and an oscillation of amplitude $\bar{A} = 0.1\bar{d}$ is shown in Fig. 6. The boundary conditions applied on the lower surface (i.e., $\bar{z} = -\bar{d}$) ensured that the director angle θ and the layer normal angle δ coincided and were both zero at that boundary. On the opposite boundary, there was a constant separation between θ and δ , corresponding to $\theta_0 - \delta_0$, and the transition between the two boundaries gives information on the realignment characteristics of the smectic-A liquid crystals in irregular domains. Unlike in the uniform domain of Sec. III,

this transition depended on the variable \bar{x} and on the domain size, as shown by values of $\theta(\bar{x}, \bar{z})$ and $\delta(\bar{x}, \bar{z})$ along different layers (i.e., different values of \bar{x}), in the different domains (Fig. 7).

In all cases, the director and layer normal vectors aligned with each other a short distance away from the upper boundary where pretilt was applied. Whereas with the same control parameters in the uniform domain where there was a symmetry in how the smectic layers and the director aligned (Fig. 4 with $\kappa = B = 1$), the realignment processes in configuration (I) displayed no such consistent symmetry for many layers. For example, along the layers $\bar{x} = 0.6\bar{L}$, and to a lesser extent along $\bar{x} = 0.2\bar{L}$, the change in the director angle θ was greater than the change in the layer normal angle δ to achieve alignment. Following their mutual alignment, both θ and δ approached zero at greater distances from the boundary. In the smallest domain, where $\bar{d} = \bar{L} = 5$, this approach to zero occurred over a shorter spatial scale than the other domains due to the influence of the lower boundary.

This configuration can be compared with that studied by de Gennes [8]. de Gennes considered a smectic-A in contact with an undulating glass surface, where the smectic planes stay locally tangent to the surface (and the molecules stay in-line with the layer normal). Assuming that the height of the local amplitude of the undulation takes the form $\alpha \cos(kx)$, where α is assumed to be small, de Gennes stated that the thickness of the distorted region was given by $l = 1/(k^2\lambda)$, where $2\pi/k$

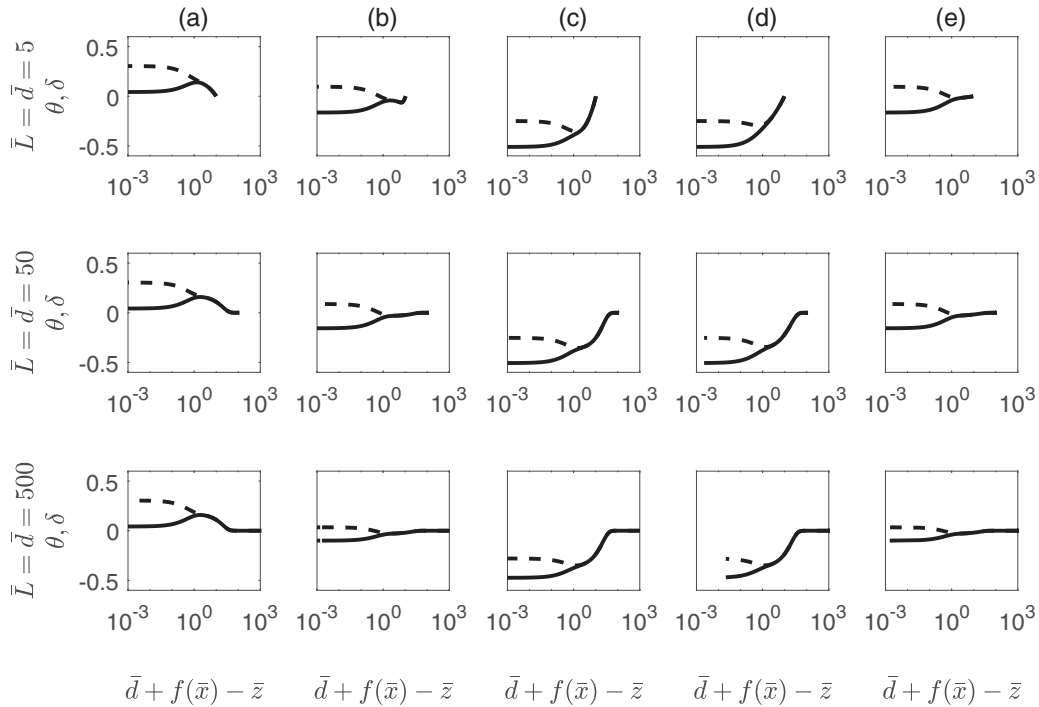


FIG. 7. The director angle $\theta(x, z)$ (solid line) and layer normal angle $\delta(x, z)$ (dashed line) are shown for numerical solutions of model equations (19) and (20) for configuration (I) in Fig. 5(a) for different size domains as indicated. Parameter values are $B = \kappa = 1$, $\bar{A} = 0.1\bar{d}$ with (a) $\bar{x} = \pm\bar{L}$, (b) $\bar{x} = -0.6\bar{L}$, (c) $\bar{x} = -0.2\bar{L}$, (d) $\bar{x} = 0.2\bar{L}$, and (e) $\bar{x} = 0.6\bar{L}$. The horizontal axes utilizes a logarithmic scale of the vertical distance from the upper surface, i.e., $\bar{d} + f(\bar{x}) - \bar{z}$.

is the wavelength of the undulation. The numerical results provided here do not show quite as large a deformation thickness as predicted by de Gennes, no doubt due to the fact that opposite boundary conditions are forcing a realignment sooner into the sample. Nevertheless, this thickness is significantly larger than the thickness of the distorted region which would be found under similar conditions with a nematic liquid crystal, which is found to be around $1/k$.

B. Configuration (II)

The numerical solutions with $B = \kappa = 1$ for the configuration shown in Fig. 5(b) using different values of \bar{d} and \bar{L} with a single oscillation of amplitude $\bar{A} = 0.1\bar{d}$ and with no phase shift between boundaries (i.e., $n = 1$, $\omega = 0$) is shown in Fig. 8.

The smaller domain $\bar{d} = \bar{L} = 5$ exhibits an interesting phenomenon absent from the larger domains; namely the existence of “bands” of molecules and layers taking similar orientations that connect the upper and lower surfaces. These “bands” essentially connect regions of the upper and lower surfaces with similar imposed values of θ and δ . However, in the larger domains, i.e., $\bar{d}, \bar{L} \geq 50$, these “bands” cease to exist and instead both the director and layer normal angles approach zero away from the boundaries; clearly demonstrating the influence of the boundaries within the sample, and the sample size itself. As before, close to the upper and lower boundaries, both θ and δ align with each another (Fig. 9) in a similar manner to that observed in configuration (I) (cf. Fig. 7).

Clearly these results in both configurations demonstrate that a rigid “bookshelf” geometry, that has been previously used throughout some mathematical investigations of the structure of smectic liquid crystals, no longer applies when boundary distortions are involved.

V. INVESTIGATION OF NONUNIFORM DOMAINS

Previous studies, e.g., Stewart [24], investigated how the structure of the smectic liquid crystals arranged in a regular “bookshelf” formation depended on the model parameters B and κ . Here we utilize a similar approach but crucially significantly extend that analysis to incorporate the role of the domain shape and the irregular boundaries of the forms introduced above. It was seen above that, except at the boundaries, the director and layer normal mutually align themselves with the horizontal and hence the impact of nonuniform domains are most evident close to the boundary. Consequently, we henceforth focus attention on the smaller domain with $\bar{d} = \bar{L} = 5$ (corresponding to $d = L = 10$ nm) where boundary contributions across the entire domain are more significant.

To quantify the overall alignment characteristics of the liquid crystal structure in response to the boundaries and model parameters, we introduce a *perturbation measure* that captures the discrepancy between the system in its lowest energy state as a result of the boundary conditions compared to that without any. In the absence of boundary conditions, as described above, the default state for the liquid crystal structure is for the director and layer normal angles to coalign with the positive \bar{x} axis, i.e., in the absence of boundary

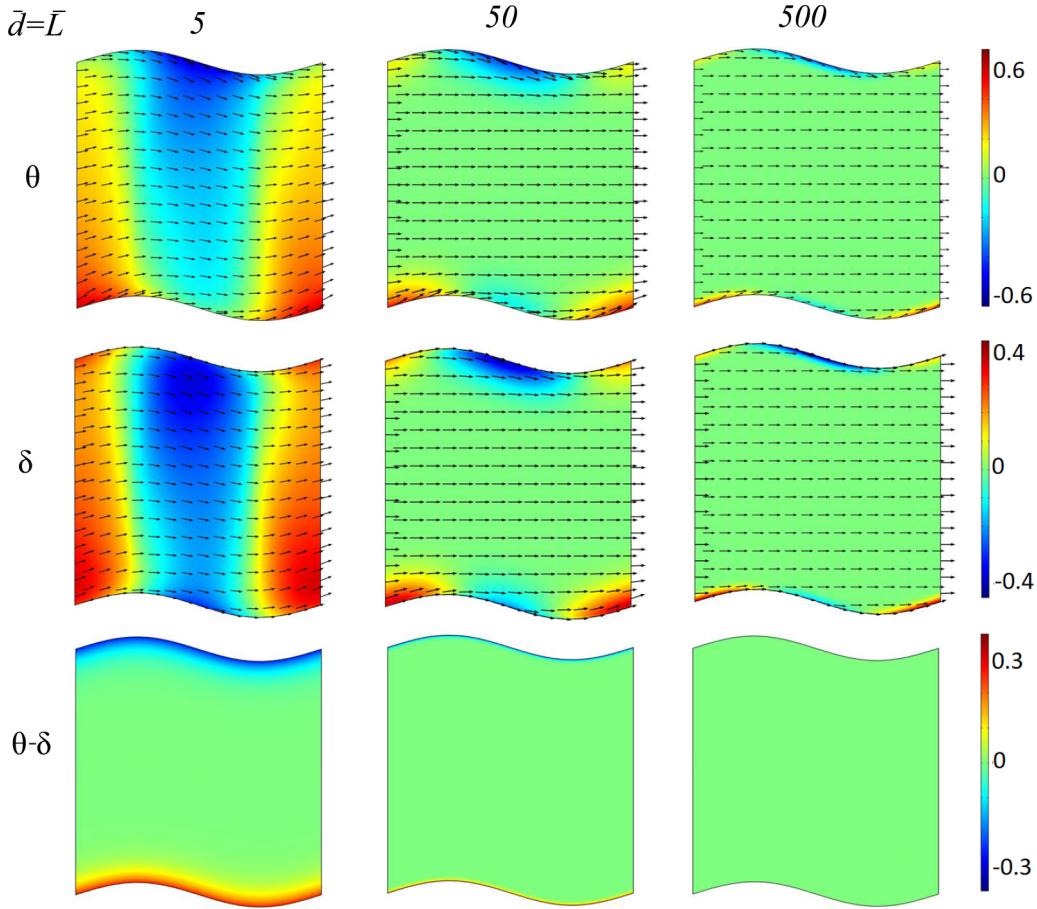


FIG. 8. Solutions of model equations (19) and (20) in configuration (II) of Fig. 5(b) for different domain sizes with $B = \kappa = 1$, $n = 1$, $\omega = 0$, and $\bar{A} = 0.1\bar{d}$ using boundary conditions as described in text with $\theta_0 = \pi/12$ and $\delta_0 = 0$ for the domain sizes indicated. The arrows indicate the director and layer normal vectors \mathbf{n} and \mathbf{a} .

conditions model equations (19) and (20) will have solution $\theta(\bar{x}, \bar{z}) = \delta(\bar{x}, \bar{z}) = 0$ for all \bar{x}, \bar{z} . Consequently, any deviation from this default state indicates the impact of boundary conditions. To quantify these deviations, we construct a normalized measure of the perturbations over the domain by introducing the integral function

$$\Omega(\xi) = \int_{-L}^L \int_{-\bar{d}+g(\bar{x})}^{\bar{d}+f(\bar{x})} \sqrt{\xi(\bar{x}, \bar{z})^2} d\bar{z}d\bar{x},$$

so that variations in the angle ξ (taken to be θ , δ , and $\theta - \delta$) over the domain are quantified by the normalized measure

$$M(\xi) = \frac{\Omega(\xi)}{\Omega(1)}, \quad (22)$$

where $\Omega(1)$ corresponds to the area of the domain. In the configurations described above, trivial integration yields $\Omega(1) = 4\bar{d}\bar{L}$.

A. Variations in the physical parameters B and κ

As the parameter B , representing the ratio of \mathbf{n} and \mathbf{a} coupling to layer compression, was increased beyond unity in both configurations, there were minimal changes in the orientation of the director angle θ but more pronounced changes in the smectic layer angle δ . However, the most

significant change was in the difference $\theta - \delta$ (Fig. 10). For $B > 1$, the director angle θ and layer normal angle δ more readily combined closer to the upper surface $\bar{z} = \bar{d} + f(\bar{x})$ resulting in a reduction of the size of the boundary layer where θ and δ differed. There was no significant change in the director or layer normal angles as B was reduced below unity in either configuration. This is expected from previous studies [25,33,34] where it was found that for small values of B , i.e., $B_0 > B_1$, the director does not realign to be parallel to the layer normal until further into the bulk of the liquid crystal sample. This is related to the minimization of the coefficient of B_0 , i.e., the minimization of $(|\nabla\Phi| + \mathbf{n} \cdot \mathbf{a} - 2)$. For large values of B , the angles defining the director and layer normal are forced to become closer in magnitude closer to the boundaries.

Variations in the parameter κ , representing the elastic properties of the sample, impacted on both the director and the layer normal angles (Fig. 11). In configuration (I), for $\kappa < 1$, both the director and layer normal angles took values close to zero only in the vicinity of the lower boundary $\bar{z} = -\bar{d}$ due to the imposed boundary conditions, whereas the pretilt applied at the upper boundary $\bar{z} = \bar{d} + f(\bar{x})$ forced these angles to take mostly nonzero values elsewhere. As κ increased, both θ and δ took values closer to zero throughout greater regions of the domain. The difference $\theta - \delta$ had a significant dependence

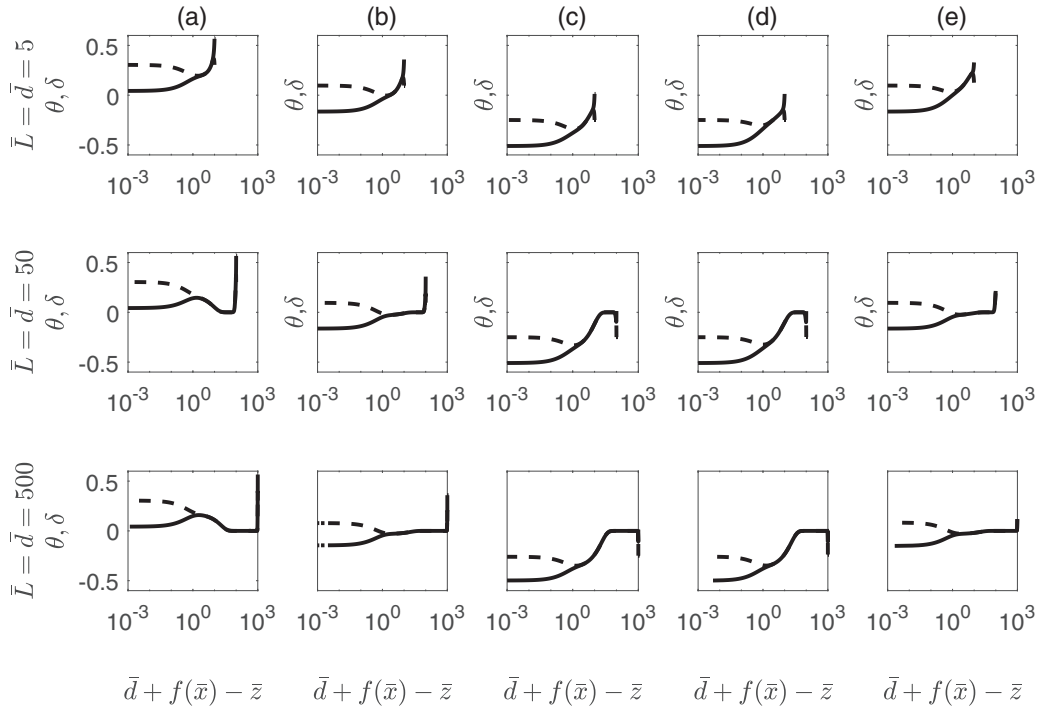


FIG. 9. The director angle $\theta(x, z)$ (solid line) and layer normal angle $\delta(x, z)$ (dashed line) are shown for numerical solutions of model equations (19) and (20) for configuration (II) in Fig. 5(b) for different size domains as indicated plotted against the vertical distance from the upper surface, i.e., $\bar{d} + f(\bar{x}) - \bar{z}$. $B = \kappa = n = 1$, $\bar{A} = 0.1\bar{d}$, $\omega = 0$ for (a) $\bar{x} = \pm\bar{L}$, (b) $\bar{x} = -0.6\bar{L}$, (c) $\bar{x} = -0.2\bar{L}$, (d) $\bar{x} = 0.2\bar{L}$, and (e) $\bar{x} = 0.6\bar{L}$.

on κ ; for small κ the layer normal and director converged close to the upper boundary $\bar{z} = \bar{d} + f(\bar{x})$ while for $\kappa > 1$ the mutual alignment arose over a greater spatial region. Again, this is somewhat expected from previous studies [25,33,34] where it was found that if κ is small, i.e., $K_1^n > K_1^a$, then the

layer angle δ increases so that the layer normal is parallel to the director and if κ is large, i.e., $K_1^a > K_1^n$, then the layers remain fixed at their boundary states until the director has reoriented to be parallel to the layer normal, they then both reorient to the equilibrium state $\delta = \theta = 0$.

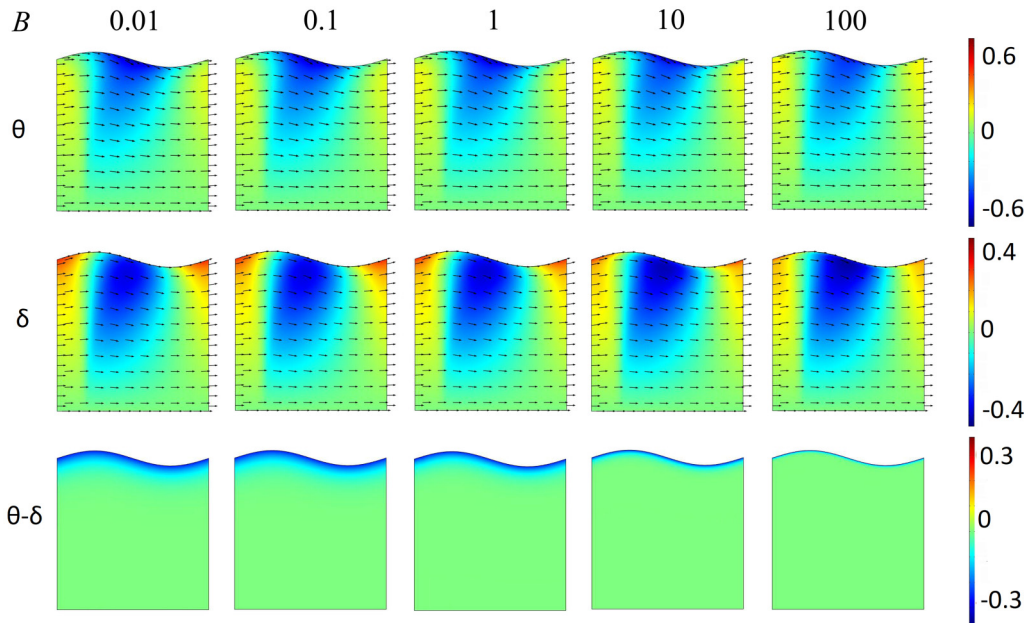


FIG. 10. Values of θ (with director \mathbf{n}), δ (with layer normal \mathbf{a}) and $\theta - \delta$ obtained from the solutions of model equations (19) and (20) for configuration (I) in Fig. 5(a) where $\bar{d} = \bar{L} = 5$, $\kappa = 1$, $\bar{A} = 0.5$, $\theta_0 = \pi/12$, $\delta_0 = 0$, and B took values as indicated.

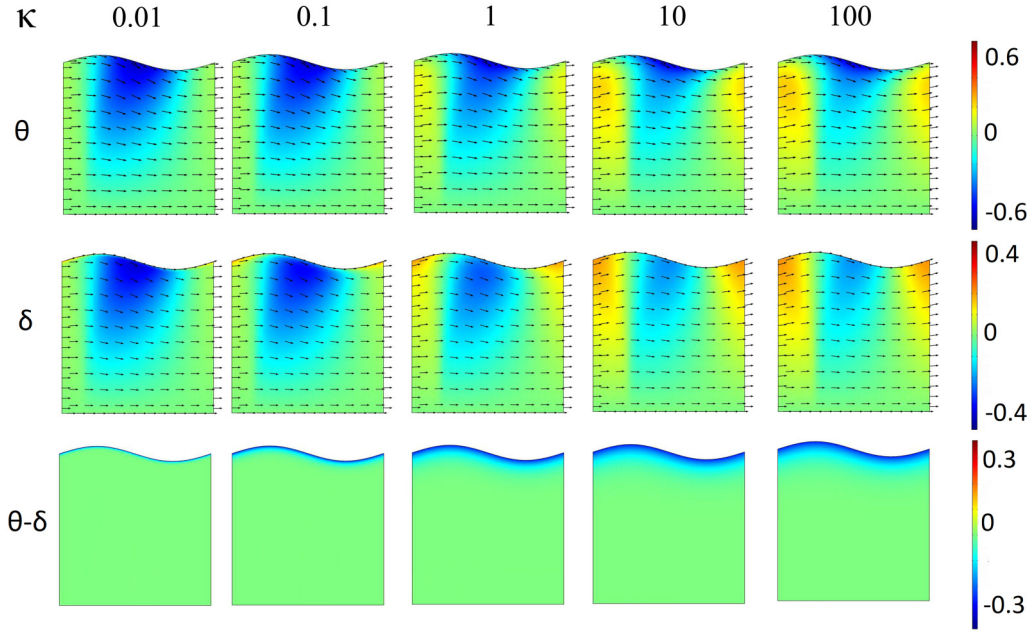


FIG. 11. Values of θ (with director \mathbf{n}), δ (with layer normal \mathbf{a}) and $\theta - \delta$ obtained from the solutions of model equations (19) and (20) for configuration (I) in Fig. 5(a) where $\bar{d} = \bar{L} = 5$, $B = 1$, $\bar{A} = 0.5$, $\theta_0 = \pi/12$, $\delta_0 = 0$, and κ took values as indicated.

The perturbation measure (22) captured the dependence of the angles θ and δ and their difference on variations of the parameters B and κ in both configurations (Fig. 12). As expected, due to the additional pretilt imposed on the lower boundary in configuration (II), $M(\theta)$, $M(\delta)$, and $M(\theta - \delta)$

were greater in configuration (II) compared to configuration (I). In both configurations, variations in the parameter B had minimal impact on either $M(\theta)$ or $M(\delta)$. However, there was a marked reduction in $M(\theta - \delta)$ as B increased from being less than unity to more than unity, quantifying the observations made in Fig. 10 concerning the mutual alignment between the layer normal and director. Again, this is an expected result and in line with previous research in the one-dimensional Cartesian “bookshelf” case [25], and the one-dimensional “cylindrical bookshelf” case [33,34]. In both configurations, increases in κ marginally reduced $M(\theta)$ and $M(\delta)$ in both configurations, suggesting that the director and layer normal align with the horizontal more readily for larger values of κ . However, increases in κ coincided with an increase in $M(\theta - \delta)$ indicating less mutual alignment between the layer normal and directors, again quantifying the graphical observations of Fig. 11. Of course, an increase in κ relates to an increase in K_1^a in relation to K_1^n , meaning that the director is more free to orient than the layers. Hence we would expect to see a larger difference in $M(\theta - \delta)$ as the director is not so constrained to be parallel to the layer normal.

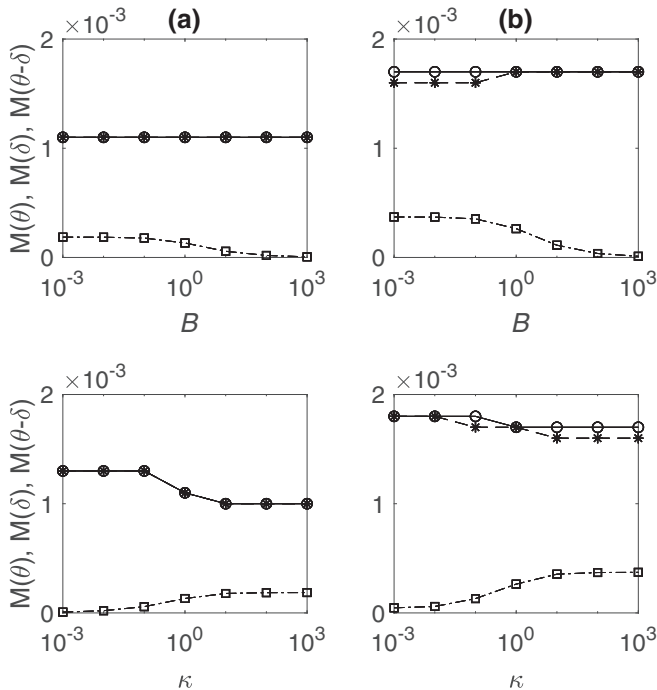


FIG. 12. The perturbation measures $M(\theta)$ (denoted by \circ), $M(\delta)$ (denoted by $*$), and $M(\theta - \delta)$ (denoted by \square) from numerical solutions of Eqs. (19) and (20) for (a) configuration (I) and (b) configuration (II) in Fig. 5 where $\bar{d} = \bar{L} = 5$, $\bar{A} = 0.5$, $n = 1$, $\omega = \pi/2$, $\theta_0 = \pi/12$, and $\delta_0 = 0$. Unless indicated, $B = 1$ or $\kappa = 1$.

B. Variations in domain structure

1. Amplitude of oscillations

Variations in \bar{A} , representing the amplitude of oscillations, had a significant impact on the alignment of the director and layer normal vectors (Fig. 13). While the director and layer normal angles changed as expected, their difference $\theta - \delta$ displayed an unexpected phenomenon as the amplitude \bar{A} increased. Specifically, differences in the distance over which θ and δ aligned close to the boundary, along with the quantitative change in their relative alignment, emerged in different layers as \bar{A} changed (Fig. 14).

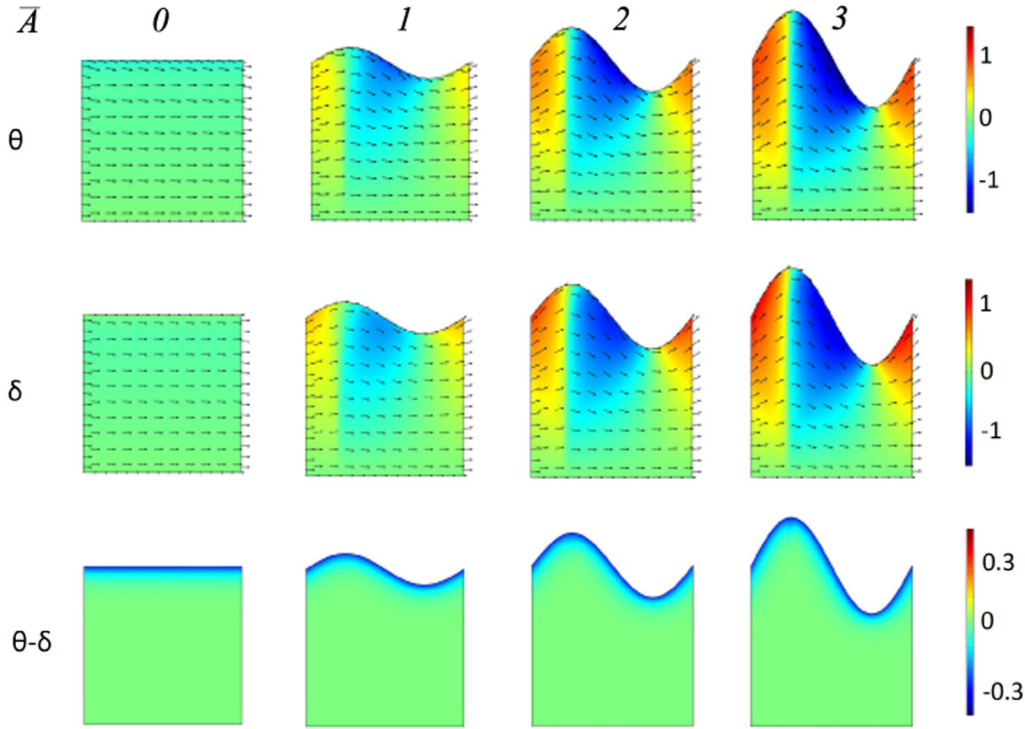


FIG. 13. Values of θ (with director \mathbf{n}), δ (with layer normal \mathbf{a}) and $\theta - \delta$ obtained from the solutions of model equations (19) and (20) for configuration (I) in Fig. 5(a), where $B = \kappa = 1$, $\theta_0 = \pi/12$, $\delta_0 = 0$, and \bar{A} took values as indicated.

The differences in the alignment characteristics between two different layers increased with the amplitude \bar{A} . When $\bar{A} = 0$, corresponding to a uniform domain, there was no difference in the relative alignment of θ and δ in different layers [Fig. 14(a)]. However, as \bar{A} increased, the differences between θ and δ depended on the layer and the differences increased with \bar{A} [Figs. 14(b)–14(d)]. Notice that the origin

of this increased alignment distance corresponds to a region in the domain that exhibits the greatest influence from boundary conditions. For illustration, consider a point in the domain with $\bar{x} = -0.5\bar{L}$ a short distance r directly below the local maximum, i.e., $(\bar{x}, \bar{z}) = (-0.5\bar{L}, \bar{d} + f(-0.5\bar{L}) - r)$ in Fig. 13. There is a significant concentration of the domain’s boundary close to this point, and thus a significant imposed discrepancy between θ and δ , and furthermore this concentration of boundaries increases with \bar{A} . Notice this boundary concentration is clearly less than at the point $(\bar{x}, \bar{z}) = (0.5\bar{L}, \bar{d} + f(0.5\bar{L}) - r)$ in Fig. 13. Consequently, the concentration of boundaries close to a surface, and therefore the curvature of the boundary, appears to play an important role in the alignment of the director and layer normal, and which may therefore explain the differences in the alignment properties shown in Fig. 14.

Intriguingly, while the perturbation measures $M(\theta)$ and $M(\delta)$ increased with \bar{A} as expected due to the increased values of θ and δ imposed at the boundaries, there was only a relatively small increase in $M(\theta - \delta)$ in either of the configurations (Fig. 15).

2. Frequency of oscillations

Variations in the oscillation frequencies of the surfaces in configuration (II) had a significant impact on the alignment of the director and layer normal vectors (Fig. 16). When the frequency of the oscillations on the upper and lower boundaries were increased, a series of “bands” were introduced connecting the upper and lower surfaces within which the director and layer normal angles were similar. These bands connected regions on opposite boundaries that had similar gradients.

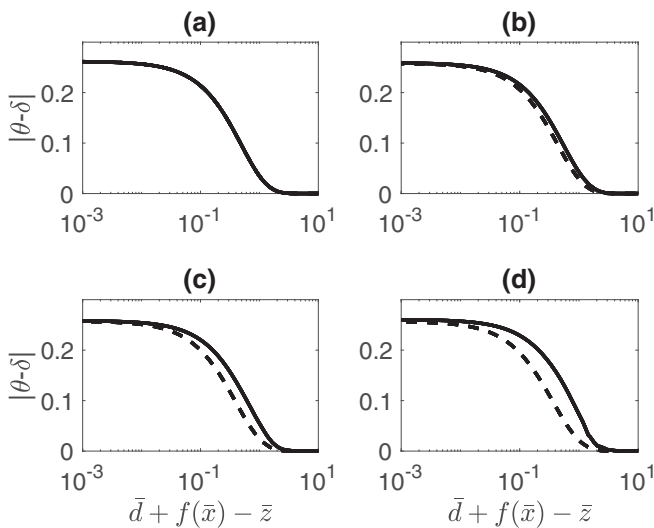


FIG. 14. Values of $|\theta - \delta|$ along $\bar{x} = -0.5\bar{L}$ (solid line) and $\bar{x} = 0.5\bar{L}$ (dashed line) as a distance from the upper surface $\bar{d} + f(\bar{x})$ obtained from the solutions of model equations (19) and (20) for configuration (I) in Fig. 5(a) with $\bar{d} = \bar{L} = 5$ where $B = \kappa = 1$, $\theta_0 = \pi/12$, $\delta_0 = 0$ and (a) $\bar{A} = 0$, (b) $\bar{A} = 1$, (c) $\bar{A} = 2$, and (d) $\bar{A} = 3$.

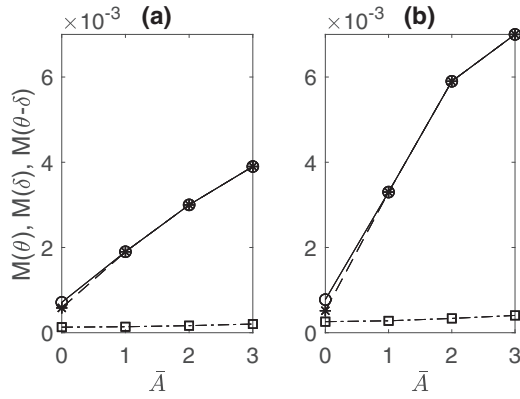


FIG. 15. The perturbation measures $M(\theta)$ (denoted by \circ), $M(\delta)$ (denoted by $*$) and $M(\theta - \delta)$ (denoted by \square) in terms of \bar{A} from numerical solutions of Eqs. (19) and (20) for (a) configuration (I) and (b) configuration (II) in Fig. 5 where $B = \kappa = 1$, $n = 1$, $\omega = \pi/2$, $\theta_0 = \pi/12$, and $\delta_0 = 0$.

Consequently, the width of these bands decreased with the frequency of the oscillations since the gradients along the boundary changed over shorter spatial scales. Moreover, the differences between the director and layer normal angles, i.e., $\theta - \delta$, displayed interesting phenomena. For large oscillation frequencies there were noticeable distortion “spikes” in the difference $\theta - \delta$ radiating into the domain originating from the local maxima on the upper surface and from the local minima on the lower surface. These “spikes” represent significant discrepancies between the director and layer normal angles not present in nearby layers and are consistent with the above observations concerning how the boundaries influence the alignment distances between the director and layer normal.

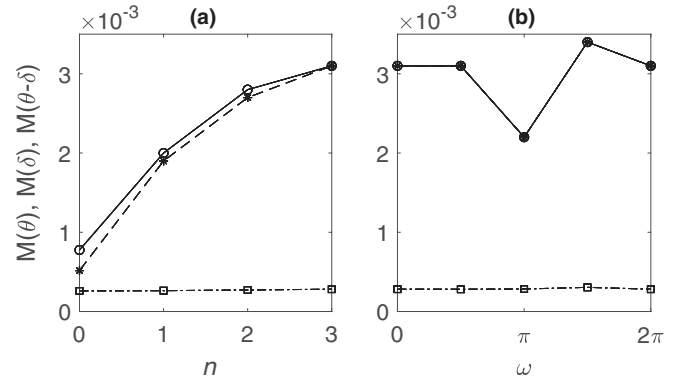


FIG. 17. The perturbation measures $M(\theta)$ (denoted by \circ), $M(\delta)$ (denoted by $*$) and $M(\theta - \delta)$ (denoted by \square) of Eqs. (19) and (20) for configuration (II) in Fig. 5(b) with $\bar{d} = \bar{L} = 5$. (a) $B = \kappa = 1$, $\bar{A} = 0.5$, $\omega = 0$, $\theta_0 = \pi/12$, $\delta_0 = 0$ and the oscillation frequency n is varied as indicated. (b) $B = \kappa = n = 1$, $\bar{A} = 0.5$, $\theta_0 = \pi/12$, $\delta_0 = 0$ and the phase shift ω is varied as indicated.

As expected, the perturbation measure applied to both the layer normal and director angles increased with the oscillation frequency n but the difference $\theta - \delta$ only underwent a small increase with n [Fig. 17(a)], suggesting that the total region in which the director and layer normal do not align was largely unaffected by n and hence the formation of the narrow “spikes” are partially canceled out elsewhere.

3. Phase shift in oscillations

It was shown above that for sufficiently large frequencies of oscillations on the upper and lower surfaces of configuration (II), “bands” connecting similar gradients on opposite

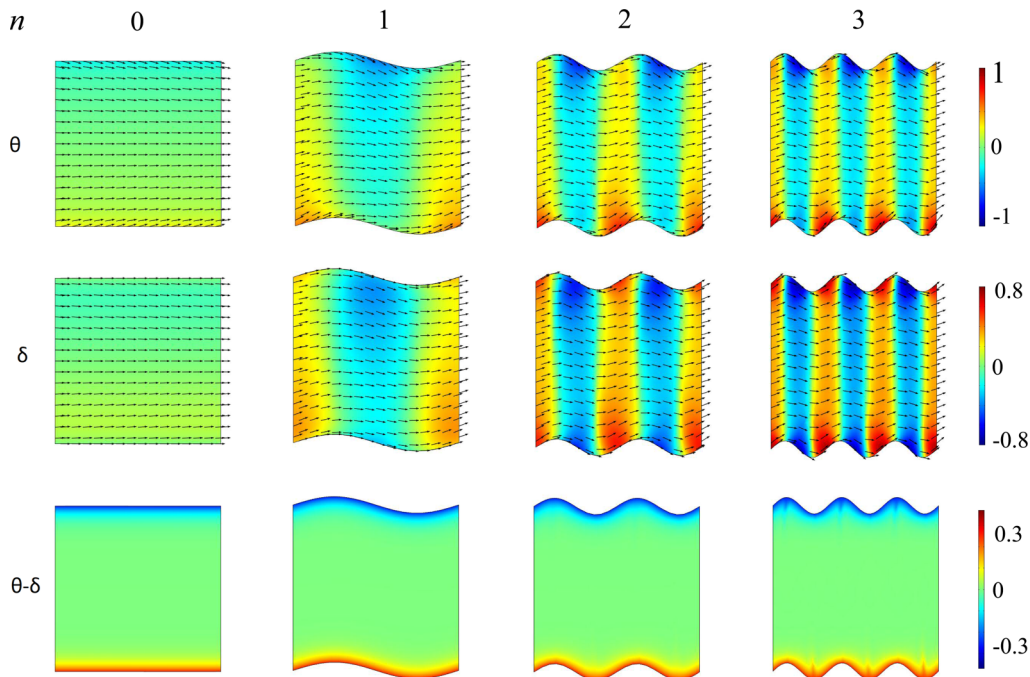


FIG. 16. Values of θ (with director \mathbf{n}), δ (with layer normal \mathbf{a}) and $\theta - \delta$ obtained from the solutions of model equations (19) and (20) for configuration (II) in Fig. 5(b) with $\bar{d} = \bar{L} = 5$, where $B = \kappa = 1$, $\bar{A} = 0.5$, $\theta_0 = \pi/12$, $\delta_0 = 0$, $\omega = 0$, and n took values as indicated.

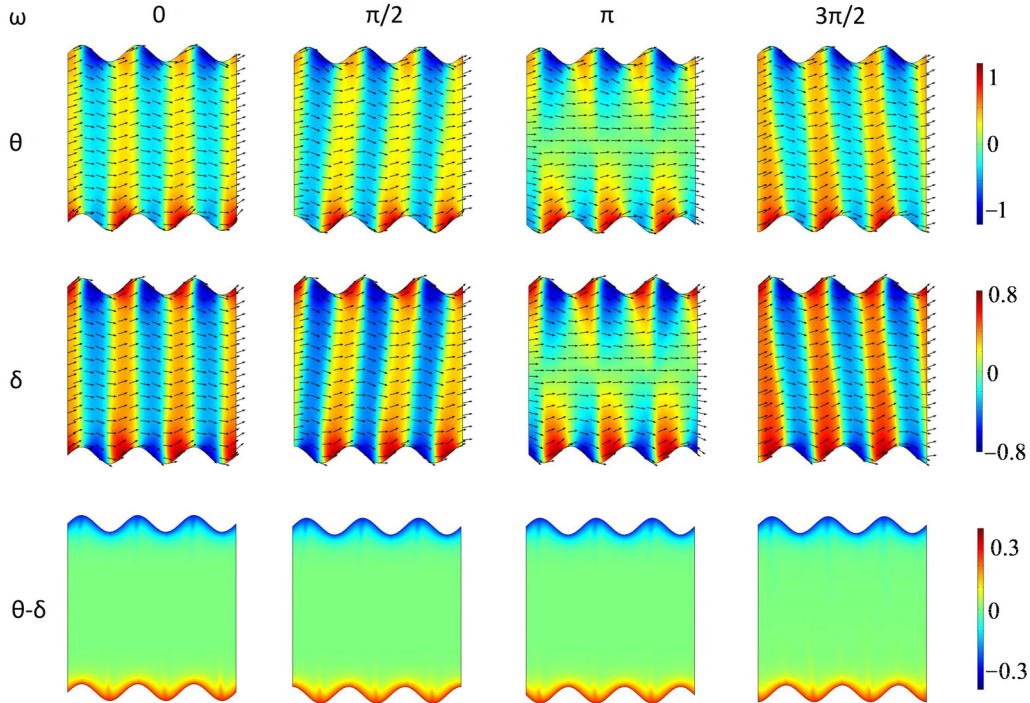


FIG. 18. Values of θ (with director \mathbf{n}), δ (with layer normal \mathbf{a}) and $\theta - \delta$ obtained from the solutions of model equations (19) and (20) for configuration (II) in Fig. 5(b) with $\vec{d} = \vec{L} = 5$ where $B = \kappa = 1$, $\vec{A} = 0.5$, $n = 3$, $\theta_0 = \pi/12$, $\delta_0 = 0$ and ω took values as indicated.

surfaces were formed within which the director and layer normal angles were similar. The orientation of these bands was naturally influenced by the phase shift ω between the upper and lower surfaces (Fig. 18). Specifically, bands in both θ and δ arose between the closest regions on opposite surfaces that exhibited similar gradients in either a positive or negative direction. The edge of these bands coincided with regions where there was a significant discrepancy between the director and layer normal, as illustrated by the previously observed “spiked” structures arising in the θ - δ plots.

The perturbation measure for both the director angle θ and layer normal angle δ changed with the phase shift ω [Fig. 17(b)]. Indeed, when $\omega = \pi$, representing a half-cycle phase shift between upper and lower boundaries, the measures $M(\theta)$ and $M(\delta)$ were minimized. Notice this particular phase shift corresponds to a symmetry in the domain when viewed along the $\vec{z} = 0$ axis, due to the pretilt applied. Changes in ω did not alter $M(\theta - \delta)$, indicating discrepancies between the director and the layer normal are local to the boundaries.

C. Discussion

A short summary of all of the investigations within this article can be found in Table I. The reorientation of the molecules and the layers seems to be highly dependent on the size of the nondimensionalized parameter B , which itself is a measure of the strength of the ratio of the coupling of the director and the layer normal to the layer compression constant. That is, when B is large (i.e., when $B_1 \gg B_0$) it would appear that the layer compression forces the molecules and layers to realign to be parallel to the x axis closer the boundaries compared to when B is small. We also find that

the size of the nondimensionalized parameter κ (the ratio of the layer splay constant to the molecule splay constant) impacts on the realignment of the director and layer normal; specifically realignment arises over shorter distances when κ is small.

However, there does not seem to be a strong immediate requirement for the director and the layer normal to align parallel to the x axis. In fact, the studies show that the molecules and layers seem to realign in order to minimize any deviation of gradients from the cell boundaries. This means that distortion spikes, which permeate through the sample for $\vec{d} = \vec{L} = 5$, are shown. The presence of these distortion spikes are highly dependent on the size of the cell boundary distortion, and the size of the cell itself, as expected. It should be noted that these distortion spikes may not necessarily correspond to a global energy minimization as, despite the variations used in the selection of the initial iterates, there is a possibility that the numerical iteration scheme used to investigate the Euler-Lagrange equations converged to a different local minimizer instead. Indeed, the existence of more than a single energy minimizer remains an interesting open problem.

These results are consistent with those found in the one-dimensional Cartesian “bookshelf” case [25] and the one-dimensional “cylindrical bookshelf” case [33]. Of course, the two-dimensional “cylindrical bookshelf” case can now be investigated using the technique described above. It will be interesting to note how important a role the radius plays in the orientation of the smectic layers and molecules.

Many more boundary structures can also now be studied. For example, boundaries which exhibit localized distortions, such as that which might appear due to dust particles on the boundary, have been studied in Ref. [54] and will appear

TABLE I. A summary of investigations.

Investigation	Results
κ decreased below unity	θ, δ boundary layers increased, $(\theta - \delta)$ boundary layer reduced δ increases toward θ , decrease in $M(\theta - \delta)$, increase in $M(\theta), M(\delta)$
κ increased above unity	θ, δ boundary layers decreased, $(\theta - \delta)$ boundary layer increased θ decreases toward δ , increase in $M(\theta - \delta)$, decrease in $M(\theta), M(\delta)$
B increased above unity	Minimal changes θ , pronounced changes in δ , minimal changes to $M(\theta), M(\delta)$ $(\theta - \delta)$ boundary layer decreased, marked reduction in $M(\theta - \delta)$
B decreased below unity	No significant changes
Addition of non-uniform boundary	Induced dependence of θ, δ on \bar{x}, \bar{L} , increased boundary layers Increased $M(\theta), M(\delta), M(\theta - \delta)$
Increase in \bar{A}	Increase in $M(\theta), M(\delta)$, small increase in $M(\theta - \delta)$
Increase in $n\pi/\bar{L}$	Increase in $M(\theta), M(\delta)$, small increase in $M(\theta - \delta)$
Changes in ω	$M(\theta), M(\delta)$ minimized at $\omega = \pi$, $M(\theta - \delta)$ unaffected.

in future publications. Further, the challenge of considering nonsmooth boundaries, such as those found in saw-tooth profiles or well geometries can now be considered for smectic-A materials, as they have been for nematics [21,56–58]. These nematic studies and many smectic studies [59–62] evidence the possibility of multi-stable states which is of particular use in bistable displays.

As mentioned, localized boundary defects have been studied in Ref. [54], using the energy minimization approach given here. Smectic-A defects have been the focus of much analytical and experimental attention, as they pose significant challenges to those who wish to use these materials in display applications [63–68]. While nonboundary defects were not considered in this work, some defects within a planar, cylindrical or spherical sample of smectic-A could also be considered using the method introduced here. Of course, defects such as dislocations and disclinations cannot be considered using this model, which assumes that layer number is constant, but must be considered by the application of parameter models such as those detailed and implemented in Refs. [67,69–72].

VI. CONCLUSIONS

In this study, we have introduced a technique for solving the nonlinear Euler-Lagrange equations associated with the free energy density of a smectic-A liquid crystal in a variety of cell designs with layer and director pretilt. For the first time in the literature, the layer normal and the director have been assumed to be functions of both the in-plane and the out-of-plane spatial variables while including a truly nonlinear layer function. We corroborated the results of Elston [38] and Stewart [24] for “bookshelf” aligned smectic-A. That is, when a uniform boundary and constant surface pretilt is applied, the orientation of the smectic layers and the director is shown to be only dependent on the in-plane spatial variable.

We then investigated nonuniform boundaries and showed that the coupling of the director and the layer normal is highly dependent on the boundary conditions applied, the spatial variables, and some of the physical properties of the liquid crystal. A number of cell designs were studied, including sinusoidal perturbations on one boundary, in-phase sinusoidal

perturbations on both boundaries, and out-of-phase sinusoidal perturbations on both boundaries. We found that, in all cases, the liquid crystal molecules and layers orient to be parallel (and hence minimize the free energy of the system) as soon into the sample as possible, while not necessarily aligning parallel to the boundaries. Consequently, throughout the bulk of the sample, i.e., except at the boundaries, since the layer normal and the director align, the free energy function (4) reduces to the form $K(\nabla \cdot \mathbf{n})^2 + B(|\nabla\phi| - 1)^2$ and so is consistent with that of de Gennes [8].

These results have immediate consequences on the use of smectic-A liquid crystals in two physical applications, namely; display technologies, and sensors. In display applications, we see that small distortions at the cell boundaries, caused by uneven plates for example, can create distortions through some of the smectic-A sample, leading to areas of nonoperability. Of course, smectic layer instabilities have been recorded previously [50,73–75], as has the difficulty with the tilt of smectic molecules with respect to boundary interfaces [8, p. 403]. However, given a smectic-A material where $B \gg 1$, these distortions can be minimized. Indeed, in sensor applications, these distortions could be used to identify roughness of a boundary, or even the introduction of a foreign body. These materials, therefore, could be used as sensors in large public spaces to detect the release of potentially dangerous molecules into the atmosphere.

While this research has considered only the static equilibrium solutions of smectic-A confined between nonuniform boundaries, there exists a further myriad of investigations to be considered by including flow regimes. Some research exists concerning Couette and Poiseuille flow of smectic-A [26,27,76,77] and flow past finite obstacles [78]; however, these have not allowed for nonlinear layer functions dependent on more than one spatial variable. Investigations of these types are paramount for investigating the material parameter value ranges which create instabilities, defects, and phase transitions, all of which which are anathema to display technologies.

This research has also allowed for a suite of further investigations that include the use of different energy densities relating to similar materials (such as other smectics), or materials with similar free-energy constructions (such as bilayer lipids).

Finally, previous research has considered the use of weak anchoring of the director on cell boundaries [32] and even free boundary conditions on the smectic layers [49] (but with the single variable dependence assumption). It remains an open problem to incorporate similar ideas to the alignment of smectic-A molecules and layers, where dependence on two spatial variables is allowed.

ACKNOWLEDGMENTS

The authors thank Prof. Nigel Mottram for extremely useful suggestions on interesting domains on which to apply our Euler-Lagrange equations. We also thank the reviewers of this paper for suggestions which have improved the validity of the model and clarity of exposition.

-
- [1] F. Reinitzer, *Monatsh. Chem.* **9**, 421 (1888).
 [2] F. Reinitzer, *Liq. Cryst.* **5**, 7 (1989).
 [3] I. W. Stewart, *The Static and Dynamic Continuum Theory of Liquid Crystals* (Taylor & Francis, London, 2004).
 [4] F. C. Frank, *Discuss. Faraday Soc.* **25**, 19 (1958).
 [5] E. G. Virga, *Variational Theories for Liquid Crystals* (Chapman & Hall, London, 1994).
 [6] J. L. Ericksen, *Arch. Ration. Mech. Anal.* **9**, 371 (1962).
 [7] J. L. Ericksen, *Phys. Fluids* **9**, 1205 (1966).
 [8] P. G. de Gennes and J. Prost, *The Physics of Liquid Crystals*, 2nd ed. (Oxford University Press, Oxford, 1993).
 [9] J. L. Ericksen, *Trans. Soc. Rheol.* **5**, 23 (1961).
 [10] F. M. Leslie, *Q. J. Mech. Appl. Math.* **19**, 357 (1966).
 [11] F. M. Leslie, *Arch. Ration. Mech. Anal.* **28**, 265 (1968).
 [12] F. M. Leslie, in *Theory and Applications of Liquid Crystals*, edited by J. L. Ericksen and D. Kinderlehrer (Springer-Verlag, New York, 1987), pp. 211–234.
 [13] F. M. Leslie, in *Theory and Applications of Liquid Crystals*, edited by J. L. Ericksen and D. Kinderlehrer (Springer-Verlag, New York, 1987), pp. 235–254.
 [14] F. M. Leslie, *Adv. Liquid Cryst.* **4**, 1 (1979).
 [15] H. J. Deuling, *Mol. Cryst. Liq. Cryst.* **19**, 123 (1972).
 [16] R. J. Atkin and F. M. Leslie, *Q. J. Mech. Appl. Math.* **23**, 3 (1970).
 [17] R. J. Atkin, *Arch. Ration. Mech. Anal.* **38**, 224 (1970).
 [18] R. J. Atkin and P. J. Barratt, *Q. J. Mech. Appl. Math.* **26**, 109 (1973).
 [19] P. Pieranski, F. Brochard, and E. Guyon, *J. Phys.* **34**, 35 (1971).
 [20] J. Walton, N. J. Mottram, and G. McKay, *Phys. Rev. E* **97**, 022702 (2018).
 [21] A. J. Davidson and N. J. Mottram, *Eur. J. Appl. Math.* **23**, 99 (2011).
 [22] I. W. Stewart, *Phys. Rev. E* **58**, 5926 (1998).
 [23] I. W. Stewart, *Liq. Cryst.* **30**, 909 (2003).
 [24] I. W. Stewart, *Contin. Mech. Thermodyn.* **18**, 343 (2007).
 [25] I. W. Stewart, *J. Phys. A: Math. Theor.* **40**, 5297 (2007).
 [26] A. J. Walker and I. W. Stewart, *J. Phys.: Condens. Matter* **21**, 155101 (2009).
 [27] A. J. Walker and I. W. Stewart, *Int. J. Eng. Sci.* **48**, 1961 (2010).
 [28] A. Contreras, C. García-Azpeitia, C. J. García-Cervera, and S. Joo, *Nonlinearity* **29**, 2474 (2016).
 [29] C. J. García-Cervera and S. Joo, *Arch. Ration. Mech. Anal.* **203**, 1 (2012).
 [30] C. J. García-Cervera and S. Joo, *J. Comput. Theor. Nanosci.* **7**, 1 (2010).
 [31] I. W. Stewart and F. Stewart, *J. Phys.: Condens. Matter* **21**, 465101 (2009).
 [32] A. J. Walker and I. W. Stewart, *J. Phys. A: Math. Theor.* **40**, 11849 (2007).
 [33] A. J. Walker, *J. Phys. A: Math. Theor.* **41**, 385205 (2008).
 [34] A. J. Walker, Theoretical studies of smectic liquid crystals subjected to flow, perturbations, magnetic fields and various applied boundary conditions, Ph.D. thesis, University of Strathclyde, 2008.
 [35] A. J. Walker and I. W. Stewart, *J. Phys.: Condens. Matter* **22**, 325106 (2010).
 [36] P. J. Collings and M. Hird, *Introduction to Liquid Crystals* (Taylor & Francis, London, 1997).
 [37] D. Coates, *Liquid Crystal Polymers: Synthesis, Properties and Applications*, Volume 118 of RAPRA Technology Limited, Rapra review reports (Shropshire, 2000).
 [38] S. J. Elston, *Liq. Cryst.* **16**, 151 (1994).
 [39] G. K. Auernhammer, H. R. Brand, and H. Pleiner, *Rheol. Acta* **39**, 215 (2000).
 [40] G. K. Auernhammer, H. R. Brand, and H. Pleiner, *Phys. Rev. E* **66**, 061707 (2002).
 [41] G. K. Auernhammer, H. R. Brand, and H. Pleiner, *Phys. Rev. E* **71**, 049901(E) (2005).
 [42] T. Soddemann, G. K. Auernhammer, H. Guo, B. Dünweg, and K. Kremer, *Eur. Phys. J. E* **13**, 141 (2004).
 [43] J. L. Ericksen, *Arch. Ration. Mech. Anal.* **4**, 231 (1960).
 [44] P. C. Martin, O. Parodi, and P. S. Pershan, *Phys. Rev. A* **6**, 2401 (1972).
 [45] P. G. de Gennes, *J. de Physique Colloque.* **30**, C4-65 (1969).
 [46] P. G. de Gennes, *Phys. Fluids* **17**, 1645 (1974).
 [47] G. Ahmadi, *J. Rheol.* **26**, 535 (1982).
 [48] W. E, *Arch. Ration. Mech. Anal.* **137**, 159 (1997).
 [49] R. De Vita and I. W. Stewart, *J. Phys.: Condens. Matter* **20**, 335101 (2008).
 [50] R. Ribotta and G. Durand, *J. Phys.* **38**, 179 (1977).
 [51] M. Kléman and O. Parodi, *J. Phys.* **36**, 671 (1975).
 [52] R. de Vita and I. W. Stewart, *Eur. Phys. J. E* **32**, 319 (2010).
 [53] R. de Vita and I. W. Stewart, *Soft Matter* **9**, 2056 (2013).
 [54] A. S. al Sallo, Mathematical modelling of smectic liquid crystals, Ph.D. thesis, University of South Wales, 2019.
 [55] COMSOL Multiphysics Reference Manual, version 5.3, COMSOL, Inc., www.comsol.com.
 [56] C. R. Evans, A. J. Davidson, C. V. Brown, and N. J. Mottram, *J. Phys. D: Appl. Phys.* **43**, 495105 (2010).
 [57] A. J. Davidson, C. V. Brown, N. J. Mottram, S. Ladak, and C. R. Evans, *Phys. Rev. E* **81**, 051712 (2010).
 [58] S. Ladak, A. J. Davidson, C. V. Brown, and N. J. Mottram, *J. Phys. D: Appl. Phys.* **42**, 085114 (2009).
 [59] H.-Y. Chen, R. Shao, E. Korblova, D. Walba, N. A. Clark, and W. Lee, *J. Soc. Inf. Display* **16**, 675 (2008).
 [60] E. A. Büyüktanir, A. Glushchenko, B. Wall, J. L. West, M. Mitrokhin, and B. Holter, *J. Soc. Inf. Display* **36**, 1778 (2005).
 [61] M. V. Mitrokhin and B. Holter, *SID Symp. Digest of Tech. Papers* **36**, 1774 (2005).
 [62] H.-Y. Chen and J.-S. Wu, *J. Soc. Inf. Display* **18**, 415 (2010).

- [63] C. D. Santangelo and R. D. Kamien, *Proc. R. Soc. A* **461**, 2911 (2005).
- [64] E. A. Matsumoto, R. D. Kamien, and C. D. Santangelo, *Interface Focus* **2**, 617 (2012).
- [65] Y. H. Kim, D. Y. Yoon, H. S. Jeong, O. D. Lavrentovich, and H.-T. Jung, *Adv. Funct. Mater.* **21**, 610 (2011).
- [66] K. J. Kidney, G. McKay, and I. W. Stewart, *Mol. Cryst. Liq. Cryst.* **438**, 263/[1827] (2005).
- [67] M. C. Calderer, C. Lui, and K. Voss, *Math. Method Appl. Sci.* **24**, 473 (2001).
- [68] I. W. Stewart, *Liq. Cryst.* **15**, 859 (1993).
- [69] H. R. Brand, P. K. Mukherjee, and H. Pleiner, *Phys. Rev. E* **63**, 061708 (2001).
- [70] N. M. Abukhdeir and A. D. Rey, *New J. Phys.* **10**, 063025 (2008).
- [71] N. M. Abukhdeir and A. D. Rey, *Liq. Cryst.* **36**, 1125 (2009).
- [72] A. Acharya and K. Dayal, *Quart. Appl. Math.* **72**, 33 (2014).
- [73] I. Dierking, M. Mitov, and M. A. Osipov, *Soft Matter* **11**, 819 (2015).
- [74] M. Delaye, R. Ribotta, and G. Durand, *Phys. Lett. A* **44**, 139 (1973).
- [75] M. Goulian and S. T. Milner, *Phys. Rev. Lett.* **74**, 1775 (1995).
- [76] M. C. Calderer and C. Liu, *Int. J. Eng. Sci.* **38**, 1007 (2000).
- [77] M. C. Calderer and B. Mukherjee, *Liq. Cryst.* **22**, 121 (1997).
- [78] H. G. Walton, I. W. Stewart, and M. J. Towler, *Liq. Cryst.* **20**, 665 (1996).